Desalination and Water Treatment
www.deswater.com

doi: 10.5004/dwt.2022.28172

250 (2022) 1–15
February

Multi-nozzle steam ejector in the MED-TVC desalination system

Xin Wang[a], Xiaoyue Zhao[a], Yulei Xing[b,*], Hongqing Lv[b], Hongkun Liu[c], Qihui Fu[d], Shenmin Xu[e], Jiaojun Xiong[e]

[a]*School of Environmental and Municipal Engineering, Tianjin Chengjian University, Tianjin 300384, China, emails: wangxchem@tcu.edu.cn (X. Wang), 1291184488@qq.com (X. Zhao)*
[b]*The Institute of Seawater Desalination and Multipurpose Utilization, MNR (Tianjin) 300192, China, emails: jobs2006@163.com (Y. Xing), lvhongqing10@163.com (H. Lv)*
[c]*China Three Gorges New Energy Co., Ltd., 100053, China, email: hsdhlhk@163.com*
[d]*Beijing Aerospace Petrochemical Technology Energy Conservation and Environmental Protection Corporation Limited, 100166, China, email: fuqh@calt11.cn*
[e]*Tianjin Innovation Technology Co., Ltd., 300384, China, emails: innovation_tj@163.com (S. Xu), xjiaojun@126.com (J. Xiong)*

Received 16 August 2021; Accepted 9 January 2022

ABSTRACT

Thermal vapor compression (TVC) is an essential part that governs the overall process in the multi-effect distillation (MED) system. A slight pressure deviation from rated primary flow condition will result in the serious performance deterioration of steam ejector. Therefore, a multi-nozzle steam ejector was proposed to solve the problem of performance deterioration under multiple unstable working conditions. A computational fluid dynamics model is used to calculate the performance of the multi-nozzle ejector under different operational conditions. The effects of both nozzle combination type and nozzle exit position (NXP) on the performance of the ejector are systematically studied. The optimal five-nozzle combination type is obtained, and the ejector entrainment ratio reaches to maximum and remains unchanged when NXP value is in the range of 0 ~ 45 mm. Following this, the devised five-nozzle steam ejector is manufactured. The performance test results demonstrate that the five-nozzle ejector has strong adaptability within a certain pressure fluctuation range of working steam. When the pressure varies from 80% to 125% of the rated pressure of primary flow, the reduction of entrainment ratio for the five-nozzle ejector is kept within 7% of the design value of the rated condition. Finally, the five-nozzle ejector is designed and used in the pilot-scale MED seawater desalination system. The five-nozzle steam ejector shows relatively stable performance with variation in primary flow pressure compared with the single nozzle ejector.

Keywords: Multi-effect distillation (MED); Steam ejector; Multi-nozzle

1. Introduction

Multi-effect distillation with thermal vapor compression (MED-TVC) is particularly more competitive and energy efficient than other thermal desalination systems due to its low energy consumption [1]. One of the major components of MED-TVC desalination system is the thermal vapor compression. TVC is usually accomplished by a steam ejector. The steam ejector entrains the secondary steam from one effect evaporator, after mixing with the working steam, the mixed steam will introduced into the first effect evaporator. This will lead to the decrease of the working steam usage [2]. Therefore, the performance of the steam ejector is vital for reducing the cost of energy and

* Corresponding author.

steam. Lots of research has been done on the design and optimization of the ejector.

El-Dessouky et al. [3] developed a semi-empirical model correlation for the complete design of the steam ejector based on large database for the primary flow pressure and the area ratio (AR). In this model, the entrainment ratio was defined as the function of the expansion ratio and the pressures of the primary flow, secondary flow and discharged flow. Zhu et al. [4] proposed a novel shock circle model for ejector performance evaluation at the critical mode operation. The proposed modeling method could predict the entrainment ratio, efficiency and coefficient of performance (COP) more accurately than those of 1D analysis methods. Eames et al. [5] proposed a design method for the supersonic streamlined steam ejector. In this design method, R245fa has been chosen as the working fluid, and it was assumed that the momentum of the mixed fluid in the diffuser chamber was uniformly changed along the axial direction. Theoretical studies have shown that the entrainment ratio and boost ratio of this steam ejector are significantly improved. Yang et al. [6] presented a semi-empirical calculation method of ejector, including calculation of the design point and variable operating condition of ejector. This calculation method was validated with the experimental data and the computational results in literatures. Therefore, the models could predict the ejector performance in a wide operating condition range of MED-TVC system. The variation in the performance of the ejector as a function of the discharge pressure for different area values of throat was given. Li et al. [7] studied the effect of AR on TVC performance by using R134a as the working fluid. They gave the quantitative relationship between AR and primary flow pressure, and also gave the quantitative relationship between AR and secondary flow pressure. Some previous investigations revealed that there exist optimum values of nozzle exit position (NXP) (the relative position of the primary nozzle exit to the inlet of the mixing chamber along the ejector axis direction, air is the working fluid) [8] and nozzle throat diameter (R134a is the working fluid) [9] at which the steam ejector could be improved significantly to the most desired entrainment performance. According to the complexity of the flow behavior inside the ejector, the mixing mechanism of the entrained vapor and motive steam are not easy to understand. A further investigation of the steam ejector is needed for the theoretical analysis.

The computational fluid dynamics (CFD) method is a useful tool for better understanding the flow behavior inside the ejector compared with conventional experimental test. Many researchers have conducted the CFD simulations on the steam ejector investigation. Fu et al. [10] used CFD simulation to study the influence of the nozzle outlet diameter and the length of the diverging section on the performance of the steam ejector. It was found that the nozzle outlet diameter has a significant influence on the entrainment ratio of the ejector. For a given operation condition, there is an optimum diameter ratio range (in their study, this range is from 1.5 to 3.5) that ensures the steam ejector acquires its best performance. Their results also show that the divergent section length of the nozzle can be designed in a much broader range than the conventional method in which the cone angle of the divergent section is limited in the range of 10°–12°. Sharifi and Boroomand [11] tried to use the two-dimensional axisymmetric CFD model to predict the steam jet ejector performance installed in a large scale MED system. It was verified that the modeling data by using the ideal gas model through CFD simulation is consistent with the experimental data. The relationship between the entrainment ratio and the structure parameters of the steam ejector was established based on CFD, and the step-by-step design method of steam ejector was proposed [12]. Furthermore, Sharifi et al. [13] developed a two-fluid model for predicting phase-changing flows inside thermal vapor compressors used in thermal desalination systems. And the TVC performance predicted by the model is more accurate than other models. Park [14] designed a basic shape of steam ejector by using the CFD method. Besides this basic shape, for the TVC design, the mixing tube diameter and the primary nozzle exit diameter are changed slightly and the change of the entrainment ratio was searched numerically when the motive and suction pressures are altered as in an actual fluctuating situation. By optimizing the throat diameter of both the ejector and primary nozzle, an improved steam ejector was obtained. And the optimized ejector could be operated in the critical mode under different operating conditions. Experimental studies by Ruangtrakoon et al. [15] showed that the nozzle geometry has a significant influence on the coefficient of performance of the steam-jet refrigeration system. Then, by using CFD method, it was found that the location of the shock wave of mixed fluid in the mixing chamber and the expansion angle of primary steam dominate the ejector performance [16]. Liu et al. [17] studied the intrinsic relationship between ejector AR and the performance of MED seawater desalination system, and established the relationship among AR, ejector efficiency and mixing efficiency. Yang et al. [18] proposed a combined numerical model to predict the supersonic non-equilibrium jetting flow inside the ejector. The effects of various operating pressures on the nozzle performance were investigated. The research explored the effect of steam pressure, temperature, supercooling level, and super-saturation ratio on the onset of the nucleation and the intensity of condensation shock in the supersonic steam flow. Wu et al. [19] found that there exist optimum convergent angle and optimum length range of mixing chamber to achieve the maximum entrainment ratio. Sriveerakul et al. [20] revealed that increasing the ejector throat length can enhance the critical back pressure, and the ejector throat length has no effect on the entrainment ratio.

Even though many works have been conducted on the steam ejector investigation at the present stage, most of them were focused on single nozzle ejector. Furthermore, because of that the steam ejector is designed on the constant operational conditions, if the characteristic parameter (such as pressure) of the working vapor is unstable, a slight pressure deviation from rated primary flow condition will result in the serious performance deterioration of steam ejector. Therefore, a multi-nozzle steam ejector was proposed to solve the problem of performance deterioration under multiple unstable working conditions.

In this article, firstly, the effects of both nozzle combination type and NXP on the performance of the multi-nozzle steam ejector were studied based on the CFD model, and

the optimized structure of multi-nozzle steam ejector was obtained. Secondly, the improved multi-nozzle steam ejector was manufactured and the corresponding performance test was performed under variable operating conditions. Finally, the multi-nozzle ejector was designed and used in a pilot-scale MED seawater desalination system. From the on-site experimental results, the multi-nozzle steam ejector can relatively perform better behavior than single-nozzle steam ejector within a pressure variation range of the primary flow.

2. MED-TVC system description

Fig. 1 shows the flow process of MED-TVC system [21]. It mainly includes the steam ejector, falling-film evaporators, condenser, and controlling devices. After preheated through the condenser and preheater, the seawater enters the first evaporator and becomes partially evaporated, then flows to the next one. The produced vapor enters into the next effect at a lower pressure and temperature than the previous effect. This vapor serves as the heating medium in the second effect. The brine from first effect enters into the second effect, and evaporates due to the vapor generated in the first effect. This process is repeated until the last evaporator, during which brine is discharged. The produced vapor inside each effect is condensed by cooling from the brine, and collected so the final distillate is obtained. The steam ejector uses the working steam (also called primary flow) to form a vacuum pressure zone, and the low pressure steam (also called secondary flow, entrained flow, etc.) is drawn from a certain evaporator. The pressure and temperature of the entrained flow is increased by mixing with the primary flow. This progress is considered as "thermal vapor compression (TVC)" which reduces the total consumption of steam.

A schematic diagram of the steam ejector is presented in Fig. 2. It mainly has five parts: nozzle, suction chamber, mixing chamber, throat, and diffuser. The typical process inside an ejector begins with high temperature and high pressure stream from the steam source, entering the ejector through the nozzle. This primary flow is accelerated and expanded to supersonic speed at the nozzle exit where it creates an aerodynamic duct to entrain the low pressure and low temperature secondary flow into the mixing chamber. The secondary flow is accelerated to sonic velocity and mixes with the primary flow in the throat. The region of supersonic

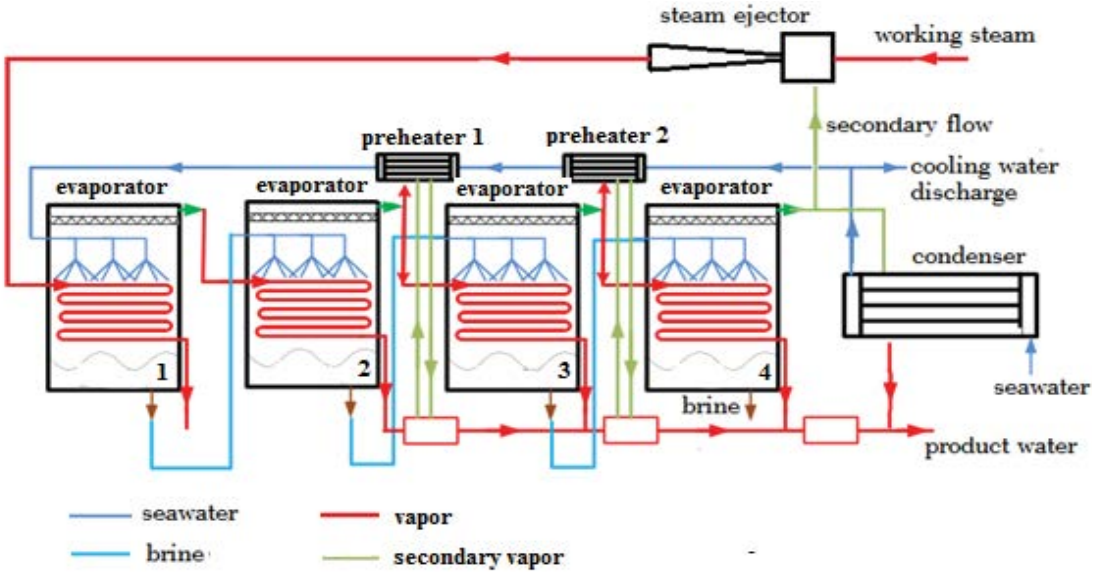

Fig. 1. Flow process of the MED-TVC system.

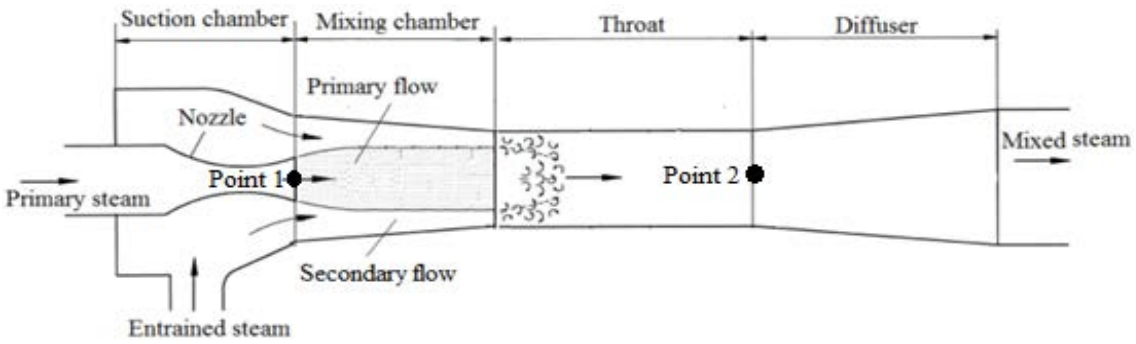

Fig. 2. Principle structure of the steam ejector.

flow is terminated by a normal shock wave further down the duct or in the diffuser.

The capacity of steam ejector is defined in terms of the flow rates of the secondary flow and the primary flow. The mixing of the primary and secondary flow mass flow rates results in the mass flow rate of the compressed vapor. As for the steam ejector performance, it can be evaluated in terms of entrainment ratio (w):

$$w = \frac{m_s}{m_p} \tag{1}$$

where m_s is the mass flow rate of the secondary flow, and m_p is the mass flow rate of the primary flow.

The flow in the ejector is usually in three modes: critical mode (with choking flow in the mixing chamber), subcritical mode (without choking flow in the mixing chamber), and malfunction mode (with reversed flow in the mixing chamber) depended on different back pressure (P_c, discharge pressure of ejector). When P_c is below the critical value (P_c^*), the entrainment ratio remains constant. When P_c is increased higher than P_c^*, the entrainment ratio begins to fall down rapidly. An ejector should be operated at the critical mode to keep steady pumping performances,

The steam ejector is a key component of MED-TVC system, and it governs the overall performance of the MED system. Considering the sensitive relationship between ejector performance and working steam condition, a further understanding of the ejector would be helpful for solving the problem of performance deterioration under the unstable condition of steam heat source.

3. Experiment setup

The experiment were carried out in the ejector performance test system. The schematic diagram of this experimental system is shown in Fig. 3. The experimental setup

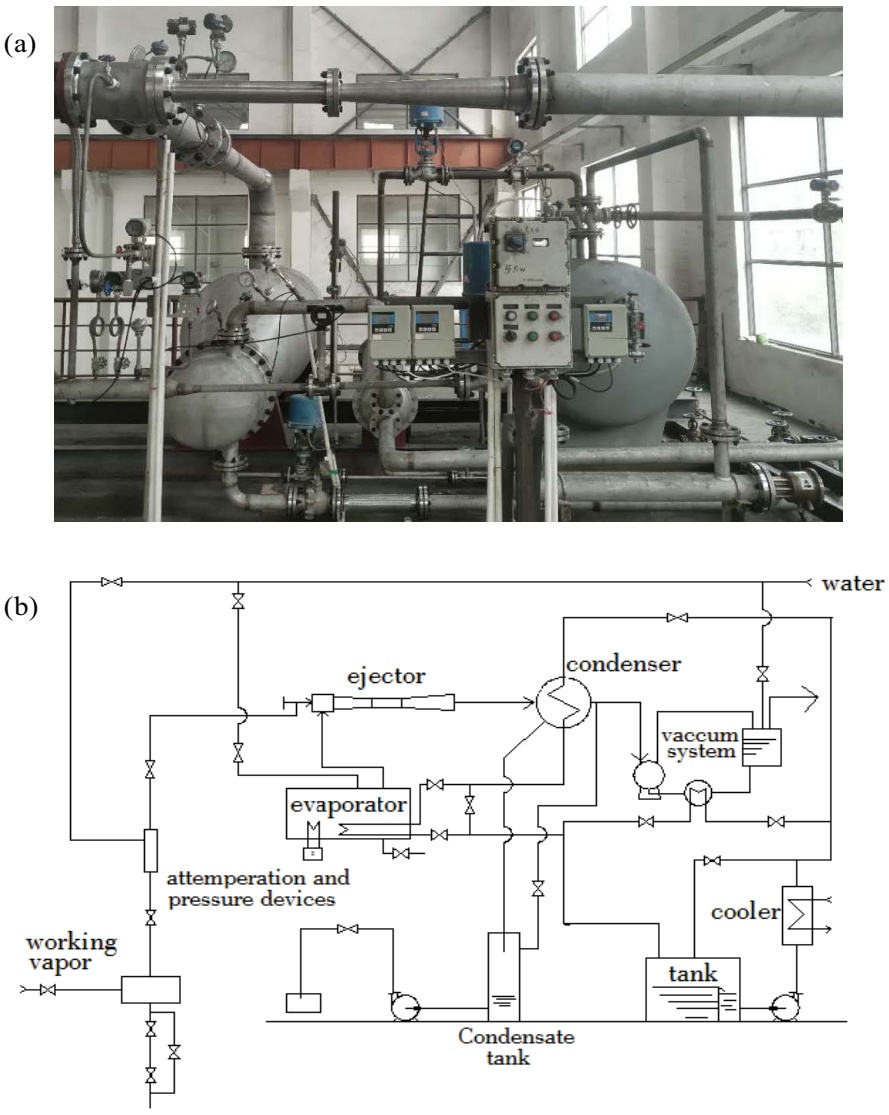

Fig. 3. Ejector performance test system: (a) experimental test system and (b) principle structure of the ejector testing system.

consisted of the evaporator, condenser, experimental ejector, vacuum system, attemperation and pressure reducing device, and etc. The primary flow was supplied by the steam boiler. After passing through the attemperation and pressure reducing device, the primary flow was adjusted to the desired pressure and temperature. The primary flow (high pressure steam) was accelerated to supersonic flow as it had passed through the nozzle. The evaporator was used to generate the water vapor for the secondary flow. Because of the low pressure region formed in the suction chamber, the secondary flow was entrained into the ejector. The primary flow and the entrained secondary flow mixed with each other in the ejector and then entered into the condenser. It should be noted here that both the evaporator and the condenser were operated under vacuum conditions, and the vacuum condition was achieved by the vacuum system connected to the condenser. The primary flow pressure (P_p) varied from 0.4 to 1.1 MPa while the secondary flow pressure (P_s) varied from 0.00959 to 0.01994 MPa (the saturation temperature corresponding to this pressure is from 45°C to 60°C).

The main purpose for doing experiments on this experimental system includes: (a) basic validation of the CFD model, (b) performance testing of multi-nozzle steam ejector. In these experiments, the temperature and pressure at the inlet of primary, secondary flow and at outlet of discharged flow were recorded. The accuracy of the pressure transducers is ±0.075%, and the accuracy of the temperature transducers is 0.1°C. The mass flow rates of steam at inlet and outlet were also measured by the mass flow meters. The working fluid used in these experiments was the saturation steam for the primary and secondary flow. The ejector used in CFD model validation experiment is the single nozzle steam ejector, and its geometrical parameters are shown in Table 1.

4. CFD model

4.1. Model description

It is obviously well known that the flow behavior inside a steam ejector is a complex, highly turbulent and supersonic speed flow. The shock waves, boundary layer separation, and high-speed airflow collisions are all existed inside the ejector. The following general assumptions are made: (1) The wall surface of the steam ejector is adiabatic. (2) The fluid flow inside the steam ejector is steady flow. (3) Both the inlets of the working steam and the entrained steam are in the dry and saturation state. The governing equations [22] for ejector modeling are described below.

Table 1
Main geometrical parameters for original single nozzle steam ejector

Geometry parameter	Value
Nozzle throat diameter (mm)	12.5
Nozzle entrance diameter (mm)	37.5
Nozzle exit diameter (mm)	29
Nozzle convergent section length (mm)	36
Nozzle throat length (mm)	8
Nozzle divergent section length (mm)	97
Mixing chamber entrance diameter (mm)	92
Mixing chamber length (mm)	349
Ejector throat diameter (mm)	62.5
Ejector throat length (mm)	250
Diffuser exit diameter (mm)	146
Diffuser length (mm)	693

- Continuity equation:

$$\frac{\partial \rho}{\partial t} + \nabla \cdot \left(\rho \vec{v}\right) = 0 \tag{2}$$

where ρ is the density, t is the time, $\vec{v}$ is the fluid velocity vector.

- Momentum equation:

$$\frac{\partial \left(\rho \vec{v}\right)}{\partial t} + \nabla \cdot \left(\rho \vec{v} \vec{v}\right) = -\nabla p + \nabla \cdot \left(\overline{\overline{\tau}}\right) \tag{3}$$

where ρ is the static pressure, $\overline{\overline{\tau}}$ is the viscous stress tensor.

The viscous stress tensor τ can be expressed as:

$$\overline{\overline{\tau}} = \mu \left[\left(\nabla \vec{v} + \nabla \vec{v}^T\right) - \frac{2}{3} \nabla \cdot \vec{v} I \right] \tag{4}$$

where μ is the molecular viscosity, I is the unit tensor, and the second term on the right hand side of above Eq. (4) represent the fluid volumetric expansion effect.

- Energy equation:

$$\frac{\partial \left(\rho E\right)}{\partial t} + \nabla \cdot \left(\vec{v}\left(\rho E + p\right)\right) = \nabla \cdot \left(k_{\text{eff}} \nabla T + \left(\overline{\overline{\tau}}_{\text{eff}} \cdot \vec{v}\right)\right) \tag{5}$$

where k_{eff} is the effective thermal conductivity coefficient ($k_{\text{eff}} = k + k_t$, where k_t is the turbulent thermal conductivity coefficient, and its specific definition depends on the used turbulence model). The two terms in the right-hand brackets of the Eq. (5) represent the energy transfer due to heat conduction and molecular viscous dissipation, respectively. E is the total energy of the fluid, it can be expressed as:

$$E = h - \frac{p}{\rho} + \frac{v^2}{2} \tag{6}$$

where h is the fluid sensible enthalpy, p/ρ is the static pressure energy, $v^2/2$ is the kinetic energy.

The governing equations mentioned above were solved numerically by using the popular commercial CFD software "ANSYS FLUENT". This CFD tool uses the control volume method to convert these partial differential equations into algebraic equations. The pressure based solver was applied to solving these governing equations, and the "standard wall function" was used for the near wall treatment.

The realizable k–ε turbulence model, which has been proved better performance to predict the jet behavior, was applied to capture the turbulent characteristics [23]. The working fluid inside the ejector was water vapor. Since the pressure of ejector working condition was relative low, the density of working fluid was calculated by using the ideal gas law. Meanwhile, the two phase flow inside the ejector was been neglected. This method has been proved by other researchers [24–26] that it is reasonable. Other properties of the working fluid are shown in Table 2. Appropriate boundary conditions were set in order to simulate the jet phenomenon inside the steam ejector. The pressure inlets were selected for working and entrained flows entering the ejector and pressure outlet was selected for the discharged flow leaving the ejector. The convergence criterion of 10^{-5} was specified for each scaled residual component of continuity, velocity components, turbulent kinetics and dissipation, and energy.

4.2. Grid independence

The accuracy of the CFD simulation is very sensitive to the number of grids used in the ejector model. The grid independent experiments of the ejector with three different number of grids were conducted. "ICEM CFD" was used to create grids for the ejector, and the number of grids were 794567, 1078542 and 1235469, respectively. By considering the most normal working conditions of the MED system, the operating parameters for the steam ejector are listed in Table 3. Those areas with large gradient of velocity and pressure are more sensitive to the grid numbers. Therefore, Point 1 and Point 2 shown in Fig. 2 were selected to verify the grid independency. Table 4 shows the modeling results for these two points at different grid numbers. As can be seen from Table 4, there is little difference in the values of velocity and pressure at Point 1 among different grid numbers. Furthermore, the differences in calculated values for pressure and velocity decrease as the number of grids increases. Considering the calculation speed and accuracy, the final grid number for the ejector simulation is 1078542 for the following ejector simulation.

Table 2
Properties of working fluid used in ejector simulation

Property	Value
Density (kg m^{-3})	Ideal gas law
Viscosity (kg m^{-1} s^{-1})	1.34×10^{-5}
Specific heat (J kg^{-1} K^{-1})	2,170
Conductivity (W m^{-1} K^{-1})	0.0261
Molecular weight (kg $kmol^{-1}$)	18.015

Table 3
The steam ejector operating conditions

Item	Absolute pressure (MPa)	Temperature (°C)
Primary flow	0.80	171
Secondary flow	0.011176	48
Discharged flow	0.03120	70

4.3. Model validation

In order to verify the CFD model mentioned above, this section used the ejector geometrical parameters from Table 1 to perform the simulation under different primary flow pressure. Fig. 4 shows the grid elements of the ejector model. The primary flow pressure varied from 0.4 to 0.8 MPa, and the secondary flow pressure was kept at the saturation pressure of 48°C. The CFD results for the entrainment ratio of the single nozzle ejector were compared to the experimental data in Fig. 5. The results show that the predicted entrainment ratio is quite close to the experimental data, with maximum relative error 7%. From these comparisons, the feasibility of the CFD method and the accuracy of the calculation model selected in this paper are verified. Therefore, the model can be used to simulate the multi-nozzle steam ejector.

5. Design method of multi-nozzle steam ejector

In order to investigate the multi-nozzle steam ejector, a series of ejectors with different number of nozzles were designed. The single nozzle steam ejector mentioned in section 3 was used as a start point for this design. According to the design idea of "Equal area criterion" (the total cross-sectional area of the nozzle throat is the same), four types of nozzle combinations in the ejector suction chamber were designed while the other parts of the ejector remained constant. Fig. 6 is a schematic diagram of the nozzle distribution of different nozzle combinations, and Fig. 7 is a two-dimensional structure of a multi-nozzle (five-nozzle) steam ejector. As can be seen from Fig. 6, A is single nozzle (d_t = 12.5 mm), B is three nozzles (d_t = 7.2 mm), C is four nozzles (d_t = 6.25 mm), and D is five nozzles (d_t = 5.6 mm). Moreover, the angle between the nozzle and the axial direction of the ejector was set to 8° for structure B, C, and D.

6. Results and discussion

6.1. Multi-nozzle steam ejector modeling

6.1.1. Effect of different nozzle combination on ejector performance

By using the operation conditions listed in Table 3 as boundary conditions, the ejectors with four structures (structure A, B, C and D) mentioned in section 5 were simulated. Table 5 shows the simulation results of corresponding entrainment ratio.

As can be seen from Table 5, under the same design conditions, the single-nozzle steam ejector has a slightly higher

Table 4
Grid independent experiment

Grid number	Pressure (Pa)	Velocity (m s^{-1})	Pressure (Pa)	Velocity (m s^{-1})
	Point 1		Point 2	
794567	10,894.78	1,037.56	18,356.42	905.47
1078542	10,940.54	1,036.63	18,756.54	867.56
1235469	10,980.65	1,039.43	18,546.43	869.75

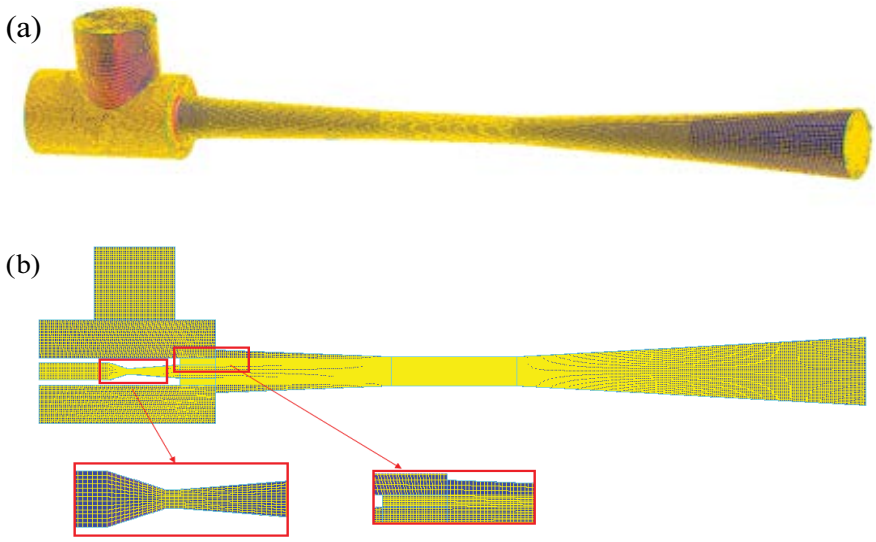

Fig. 4. Calculation domain and mesh of the ejector CFD model: (a) mesh for the overall structure of the ejector and (b) mesh for the cross-section of the ejector.

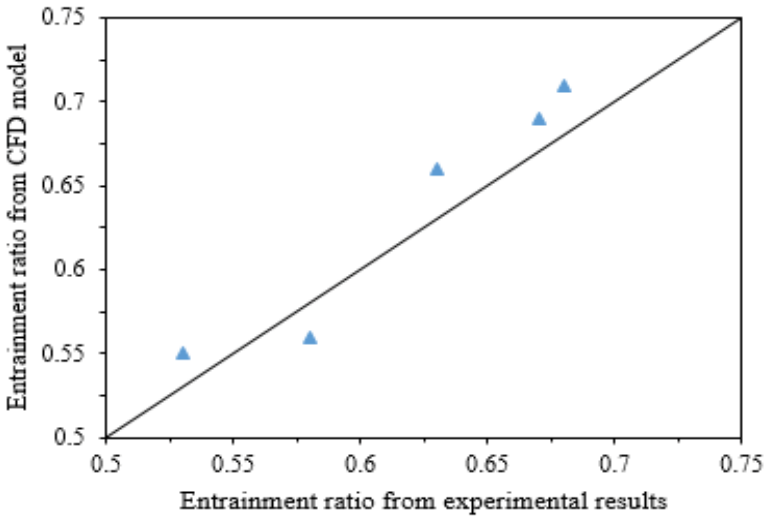

Fig. 5. Comparison of simulation result with experimental data.

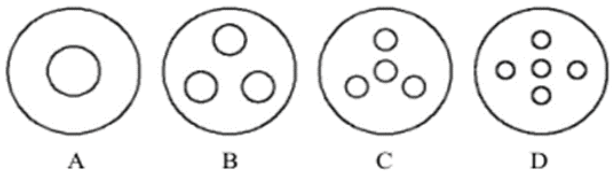

Fig. 6. Nozzle distribution for different nozzle combination.

entrainment ratio, followed by five nozzles (D), four nozzles (C), and three nozzles (B). Among them, the three nozzles (B) has a relative larger difference on the ejector entrainment ratio compared with the other three nozzle combinations. The reason for this phenomenon can be explained by Fig. 8. On the one hand, the size of three nozzles (B) are larger compared with C and D, the energy loss due to collision at the tails of the three working steam is large; for the C and D structures, there exist a primary nozzle on the ejector central axis, the energy of shock wave chain produced in the working steam is more than that of other nozzles distributed around it, so that the energy loss due to collision at the tail of each working steam is small. On the other hand, the arrangement of the three-nozzle structure affects the effective cross-sectional flow area of the ejector for sucking vapor into the ejector, which results in the decrease in the ejector entrainment ratio.

In addition, compared with C structure, the overall energy intensity of the shock wave chain for the D structure is stronger and it has a long range of influence. Therefore, the ejector entrainment ratio of D structure (five-nozzle steam ejector) is relatively large.

Through the above analysis, apart from the single nozzle (structure A), the optimal multi-nozzle combination is the five-nozzle combination shown in structure D.

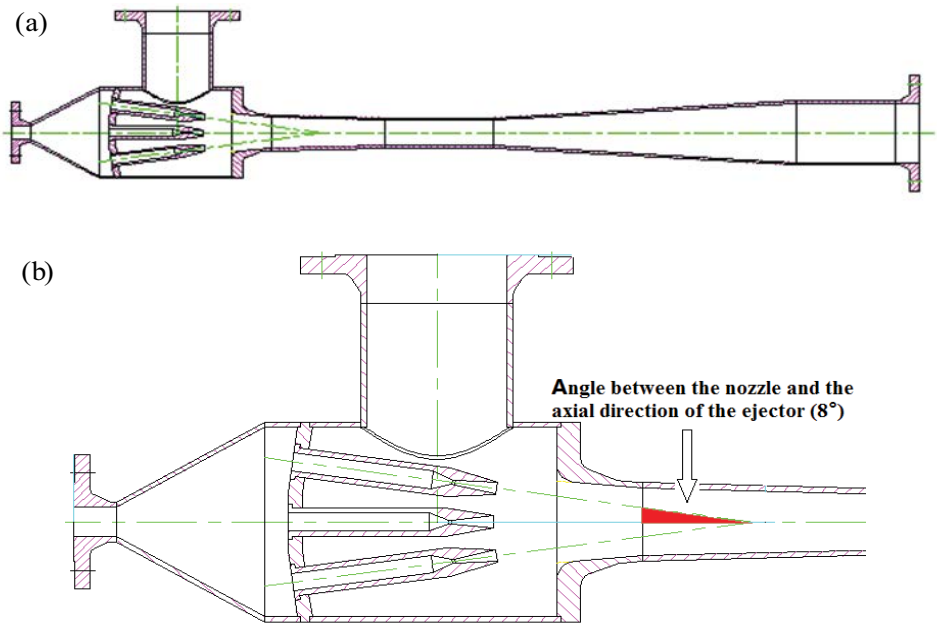

Fig. 7. Structure diagram of five-nozzle steam ejector: (a) five-nozzle steam ejector and (b) angle between the nozzle and the axial direction of the ejector.

Table 5
Effect of nozzle combination on ejector entrainment ratio

	w
Single nozzle (A)	0.8021
Three nozzles (B)	0.6575
Four nozzles (C)	0.7643
Five nozzles (D)	0.7918

6.1.2. Effect of NXP on ejector performance

The nozzle exit position (NXP) is one of the most important parameters influencing the performance of the ejector. Since the jet zone in the multi-nozzle ejector is similar to a cone, unlike a single nozzle ejector in which the jet zone is cylindrical, the flow field of the multi-nozzle steam ejector is more complicated than that of the single nozzle ejector. In order to investigate the relationship between the NXP and the flow field in the five-nozzle steam ejector, the corresponding numerical simulation were carried out for NXP = –90, –75, –60, –45, –30, –15, 0, 15, 30, 45 mm (the value of NXP at the inlet of the mixing chamber is defined as zero, the left side of NXP = 0 mm is negative, and the right side of NXP = 0 mm is positive). The simulation were performed under the working conditions listed in Table 3, and the simulation results are shown in Figs. 9 and 10.

Fig. 9 shows the effect of NXP on the entrainment ratio of the five-nozzle steam ejector. Near the entrance region of the mixing chamber, as the NXP moves from left to right, the entrainment ratio increases firstly and then remains constant. The farther the nozzle exit from the entrance of the mixing chamber, the smaller the entrainment ratio is. Within the allowed range of ejector structural dimensions, the entrainment ratio remains substantially unchanged as the nozzle exit moves to the right within a certain distance in the mixing chamber.

The reasons for the phenomenon shown in Fig. 9 can be explained as follows: the kinetic energy for the secondary flow entering the ejector is mainly achieved from the primary flow. The secondary flow obtains the kinetic energy during the energy exchange with the primary flow. When the value of NXP is relatively small, since the diameter of the suction chamber is much larger than the entrance diameter of mixing chamber, the low pressure zone where the nozzle outlet is located is relatively large. This large low pressure zone will lead to the rapid energy loss of primary flow. So that the primary flow can only participate in the energy exchange process with the secondary flow at a lower energy intensity. The energy obtained by the secondary flow is reduced, and the corresponding entrained flow rate is decreased. So the ejector entrainment ratio is reduced. With the NXP value increases, it can be seen from Fig. 10 that the energy intensity of the primary flow entering the mixing chamber is increased, which makes the energy exchange between the primary and the secondary flow more completely. The kinetic energy obtained by the secondary flow increases, the corresponding flow rate of entrained flow increases accordingly, and the ejector entrainment ratio increases. However, as the NXP continues to increase, the position of the five nozzles has a negative effect on the effective flow cross-sectional area of the secondary flow, which will not be in favor of entering the mixing chamber for the secondary flow. At the same time, the kinetic energy obtained by the secondary flow makes it sufficient to reach to the sonic or even supersonic conditions, choking occurs in the ejector throat section, and the flow rate of the entrained flow reaches to the maximum and remains constant. Therefore, there is an optimum NXP range for the five-nozzle ejector. When the NXP value is in the range of

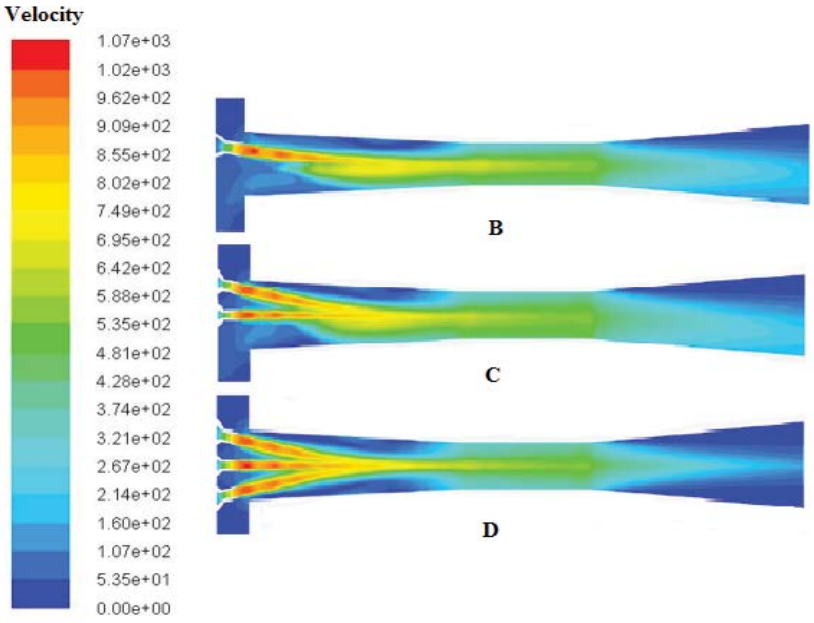

Fig. 8. Contours of flow field of structure B, C and D.

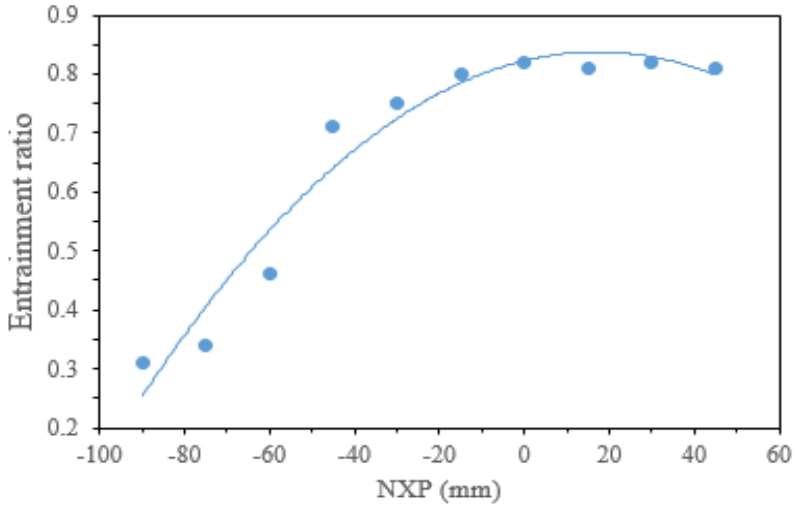

Fig. 9. Effect of NXP on the entrainment ratio of five-nozzle ejector.

0 ~ 45 mm, the ejector entrainment ratio remains basically the same.

6.1.3. Performance comparison between multi-nozzle and single-nozzle ejector

For a conventional single-nozzle steam ejector, when the operating conditions deviate from the design value, the ejector performance will be severely deteriorated. In order to investigate the influence of primary flow pressure on ejector performance, this section compared the five-nozzle steam ejector with a single-nozzle steam ejector under the operating conditions listed in Table 6.

From the perspective of the ejector entrainment ratio, Fig. 11 shows that the five-nozzle steam ejector behaves some advantages compared to the single-nozzle steam ejector. The entrainment ratio of five-nozzle steam ejector fluctuates within the range from 0.69 to 0.80 when the working vapor pressure is 0.5–1.0 MPa, and it can be kept relatively high and stable. While for the single-nozzle steam ejector, with the increase of working steam pressure, the entrainment ratio firstly increases gradually. When the working steam is 0.8 MPa, the entrainment ratio reaches to the maximum value, then decreases gradually. The entrainment ratio of single-nozzle ejector varies from 0.59 to 0.82.

The reason for these results shown in Fig. 11 is as follows: when the five-nozzle steam ejector is working under the low pressure of primary flow, the multiple working steam can increase the contact area with the entrained steam, and the ability to entrain the steam of the shock wave

boundary layer is increased. So it is beneficial to increase the entrainment ratio. With the increase of primary flow pressure, the diameter and length of the shock wave chain after the nozzle becomes larger and longer. But due to the splitting effect of the five-nozzle on the working steam, the variation of the shock wave chain produced in the working steam at each nozzle outlet is small, so the entrainment ratio does not change greatly. For a single nozzle steam ejector, when the primary flow pressure is relatively low, because of the small energy intensity of the shock wave chain, the ability to attract the secondary steam is small. The small capacity of steam attraction results in a small entrainment ratio. When the primary flow pressure is high, the increase in the diameter of the shock wave directly affects the effective flow cross-sectional area when the entrained vapor enters the mixing chamber. And this leads to a decrease in the ejector entrainment ratio. In the practical engineering application, the working steam pressure may be affected by the outside circumstance. The five-nozzle steam ejector can maintain

Table 6
Ejector working conditions

Item	Absolute pressure (MPa)	Temperature (°C)
Primary flow	0.50–1.20	Saturation temperature
Secondary flow	0.011176	48
Discharged vapor	0.03120	70

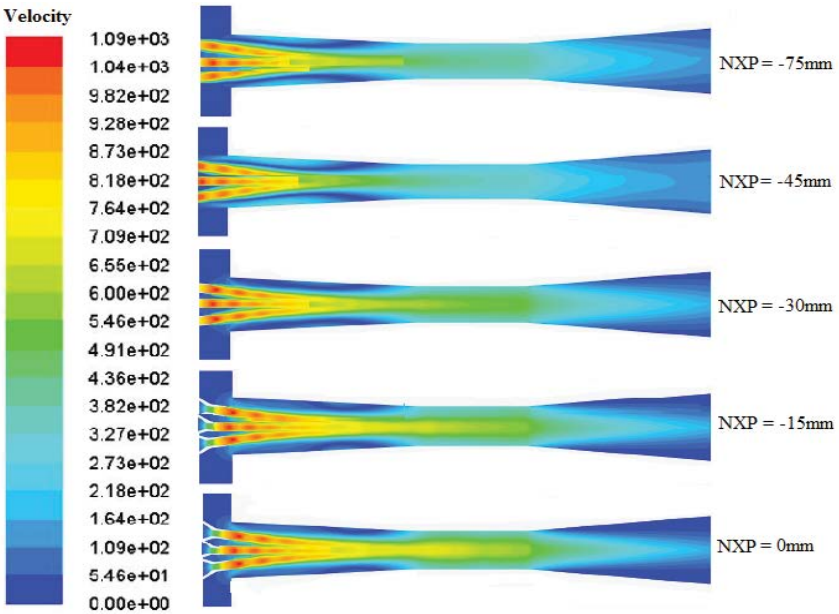

Fig. 10. Flow field in a five-nozzle steam ejector with different NXP.

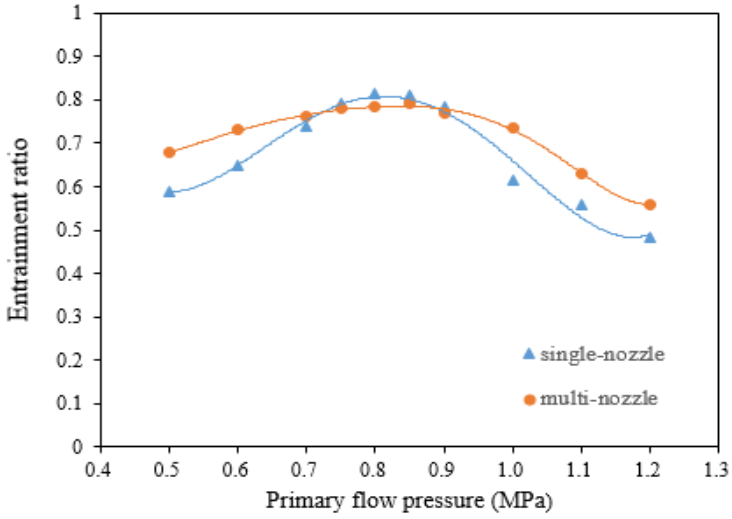

Fig. 11. Effect of working steam pressure on the entrainment ratio of ejector.

relatively stable performance, which will be of great significance to the stable operation of the entire MED-TVC system.

6.2. Experimental testing

According to the CFD calculation results of the multi-nozzle ejector in the above section, the optimized five-nozzle steam ejector was designed and processed. The geometric parameters of the five-nozzle steam ejector are listed in Table 7. In order to test the practical performance of this five-nozzle steam ejector, the performance measurements were carried out in our experimental system. This experiment testing considered various primary flow pressure of P_p = 0.4, 0.5, 0.6, 0.65, 0.7, 0.75, 0.80, 0.9, 1.0, 1.1 MPa. In all cases, the secondary flow pressure P_s was kept close to the saturation pressure of 48°C, and the back pressure P_c was about 0.034 MPa. The detailed experimental data for the five-nozzle steam ejector are listed in Table 8.

Fig. 12 shows the experimental results for the entrainment ratio of five-nozzle ejector under different primary flow pressure. For this five-nozzle ejector, the rated design condition of the primary flow pressure is 0.8 MPa, and the average value of the tested entrainment ratio is 0.82. When

Table 7
Main geometrical parameters for the five-nozzle steam ejector

Geometry parameters	mm
Nozzle throat diameter (mm)	5.6
Nozzle entrance diameter (mm)	20
Nozzle exit diameter (mm)	14
Nozzle convergent section length (mm)	21
Nozzle throat length (mm)	3
Nozzle divergent section length (mm)	44
Mixing chamber entrance diameter (mm)	92
Mixing chamber length (mm)	349
Ejector throat diameter (mm)	62.5
Ejector throat length (mm)	250
Diffuser exit diameter (mm)	146
Diffuser length (mm)	693

Table 8
Experimental data for the five-nozzle steam ejector

P_p (MPa)	T_p (°C)	P_s (MPa)	T_s (°C)	P_c (MPa)	T_c (°C)	m_p (kg h^{-1})	m_s (kg h^{-1})	w
0.402	143.79	0.0112	48.06	0.031	88.67	58	25	0.431
0.398	143.43	0.0111	48.58	0.034	89.34	57	23	0.404
0.402	143.80	0.0112	48.72	0.032	88.99	58	26	0.448
0.498	151.69	0.0109	48.04	0.031	89.75	112	79	0.705
0.492	151.32	0.0109	47.89	0.032	89.12	112	78	0.696
0.501	151.91	0.0108	47.99	0.034	90.03	114	75	0.658
0.601	158.89	0.0110	48.01	0.031	90.02	162	120	0.741
0.602	158.91	0.0109	48.23	0.032	89.12	162	127	0.784
0.606	158.86	0.0111	48.14	0.034	89.56	163	130	0.798
0.652	162.15	0.0112	47.87	0.034	88.98	226	179	0.792
0.651	162.11	0.0111	48.05	0.034	88.78	227	188	0.828
0.653	162.15	0.0111	48.68	0.032	89.97	230	189	0.822
0.701	165.01	0.0118	47.89	0.034	90.05	295	243	0.824
0.701	165.03	0.0116	47.98	0.032	88.74	295	245	0.831
0.701	165.03	0.0113	48.23	0.032	89.34	295	232	0.786
0.753	167.92	0.0112	47.98	0.032	89.03	379	310	0.818
0.752	167.92	0.0110	48.45	0.034	90.24	379	314	0.829
0.752	167.92	0.0111	48.09	0.034	88.74	379	301	0.794
0.801	170.48	0.0112	48.65	0.034	89.43	454	362	0.797
0.801	170.49	0.0111	47.55	0.032	89.46	453	372	0.821
0.802	170.51	0.0111	47.87	0.032	89.51	453	372	0.821
0.898	175.27	0.0112	47.98	0.032	88.76	605	484	0.800
0.901	175.43	0.0108	48.45	0.034	90.02	605	493	0.815
0.901	175.45	0.0107	48.12	0.032	90.12	605	476	0.787
1.001	179.98	0.0108	46.77	0.032	89.12	760	578	0.761
1.002	179.96	0.0110	47.79	0.031	89.56	761	560	0.736
1.002	179.99	0.0111	48.02	0.033	89.56	760	579	0.762
1.101	184.13	0.0112	48.34	0.034	89.76	924	650	0.703
1.102	184.56	0.0106	47.17	0.033	90.34	923	669	0.725
1.101	184.76	0.0107	48.56	0.034	90.21	923	671	0.727

the pressure varies from about 80% to 125% of the rated design condition (i.e., 0.6–1.0 MPa), the reduction of entrainment ratio for the five-nozzle ejector is kept within 7.5% of the design value of the rated condition (i.e., entrainment ratio varies from 0.76 to 0.82). Because of that there is little reduction in the entrainment ratio, the variation range from 80% to 125% of the rated primary pressure is called as "stable working zone" for the five-nozzle ejector. Therefore, the five-nozzle ejector can behave relatively stable performance when the primary flow pressure varies in the "stable working zone".

6.3. Multi-nozzle steam ejector for pilot scale MED system

Based on the above research, a five-nozzle steam ejector was applied to the 50 m^3 d^{-1} MED seawater desalination system. This MED system shown in Fig. 13 is located in Shandong Lubei Power Plant. It mainly includes 7 effect evaporators, steam ejectors, and 1 condenser. The feed configuration of this MED system is the counter-current grouping feed scheme. The 7 effect evaporators are divided into two groups: 1st–3rd and 4th–7th effect evaporators. The seawater enters the effect of the last group (4th–7th effect evaporators), and is heated to boiling point, during which some seawater is vaporized. The remaining seawater is repeatedly heated and vaporized in the next group of evaporators (1st–3rd effect evaporators). The suction position of ejector is located on the last effect. By considering the steam source and MED working conditions, the ejector design parameters were determined and listed in Table 9. At the same time, a single nozzle steam ejector shown in Fig. 14 is also equipped on the MED system for comparison with the multi-nozzle steam ejector.

Comparative experiments between five-nozzle steam ejector and single-nozzle steam ejector were carried out on this MED pilot plant to investigate the effect of primary flow pressure variation on its performance. In these experiments, the temperature and pressure at the inlet of primary, secondary flow and at outlet of discharged flow were recorded, and the mass flow rates of steam at inlet and outlet

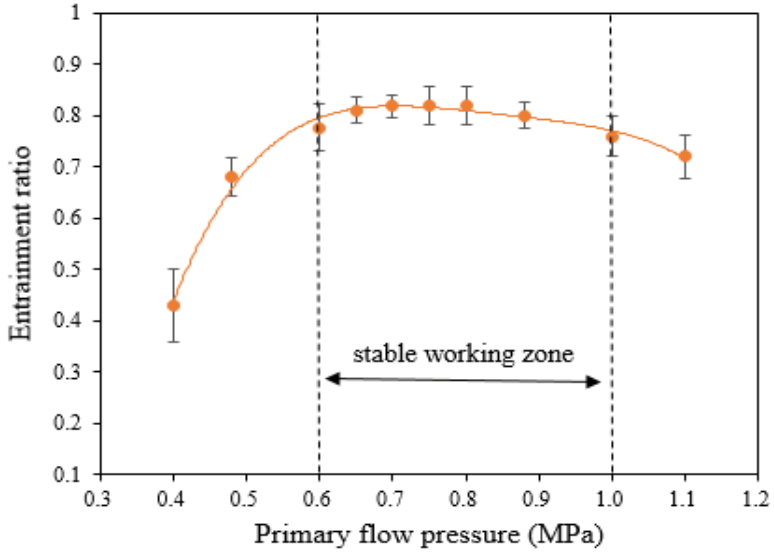

Fig. 12. Effect of primary flow pressure on entrainment ratio of five-nozzle ejector. Error bars represent the standard deviations of duplicate measurements.

Fig. 13. 50 m^3 d^{-1} MED-TVC pilot plant in Shandong Lubei Power Plant.

of the ejector were measured by the vortex flow-meter. The primary flow pressure varied from 0.48 to 1.0 MPa, and the secondary flow pressure was kept close to the saturation pressure of 51°C (i.e., saturation pressure was 0.01248 MPa). Fig. 15 shows the experimental results for the comparison of entrainment ratio under different primary flow pressure.

As shown in Fig. 15, from the perspective of the entrainment ratio, the single-nozzle steam ejector can maintain the entrainment ratio above the value of 0.80 in the primary flow pressure range of 0.75~0.80 MPa. However, when the pressure fluctuation of primary flow exceeds this range, the entrainment ratio will decrease sharply. For the five-nozzle steam ejector, the relatively high and stable entrainment ratio can be maintained over a wide range of primary flow pressure (0.6~0.9 MPa). When the primary flow exceeds this pressure fluctuation range, there is smaller decrease in the entrainment ratio for the five-nozzle steam ejector than that of the single-nozzle steam ejector. Therefore, the multi-nozzle steam ejector proposed in this paper can fully meet the application requirements within a certain pressure variation range of the primary flow.

Table 9
Ejector design parameters

Item	Absolute pressure (MPa)	Temperature (°C)
Primary flow	0.78	170
Secondary flow	0.01248	51
Discharged flow	0.034	92

7. Conclusion

In this paper, CFD method was used to systematically investigate the multi-nozzle steam ejector in the MED desalination system. On the one hand, the multi-nozzle steam ejector was designed and optimized. On the other hand, the entrainment performance comparison between

Fig. 14. Steam ejectors used in 50 m^3 d^{-1} MED pilot plant.

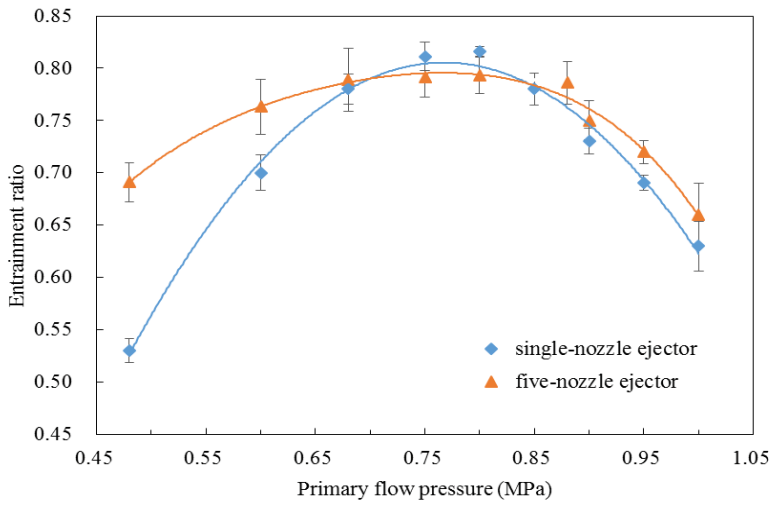

Fig. 15. Experimental measurement of the average and standard deviation of the entrainment ratio under different primary flow pressure. Error bars indicate the standard deviations.

the single-nozzle and multi-nozzle steam ejector under the same operating conditions was conducted. The following conclusions were made:

- For the multi-nozzle steam ejector, there exist optimum nozzle combination type and NXP. The optimal five nozzles combination type and an optimum NXP range are obtained. When the NXP value is in the range of 0 ~ 45 mm, the ejector entrainment ratio remains basically the same.
- Under the same operating conditions, compared with the single-nozzle steam ejector, the five-nozzle steam ejector can maintain a relatively high entrainment ratio when the primary flow pressure fluctuates. When the pressure varies from 80% to 125% of the rated pressure of primary flow, the reduction of entrainment ratio for the five-nozzle ejector is kept within 7% of the design value of the rated condition.
- A five-nozzle steam ejector is designed for 50 m^3 d^{-1} pilot scale MED seawater desalination device. According to the results of on-site commissioning, compared with the single nozzle ejector, the five-nozzle steam ejector designed in this paper shows relatively stable performance with variation in primary flow pressure.

Acknowledgments

The work was funded by Tianjin Technical Cooperation R&D and Industrialization Projects for the Belt and Road Initiative (18YDYGHZ00100). And the numerical simulation in this work was supported by the high-performance computing platform of Tianjin Chengjian University.

Symbols

h	—	Sensible enthalpy of fluid, J
I	—	Unit tensor,
m_p	—	Mass flow rate of primary flow, kg h^{-1}
m_s	—	Mass flow rate of secondary flow, kg h^{-1}
p	—	Static pressure, Pa
P_c	—	Absolute pressure of mixed(discharged) flow, MPa
P_p	—	Absolute pressure of primary flow, MPa
P_s^p	—	Absolute pressure of secondary flow, MPa
t	—	Time, s
T_c	—	Temperature of mixed flow, °C
T_p	—	Temperature of primary flow, °C
T_s^p	—	Temperature of secondary flow, °C
w	—	Entrainment ratio
ρ	—	Density, kg m^{-3}
$\vec{\bar{v}}$	—	Fluid velocity vector, m s^{-1}
τ	—	Viscous stress tensor
k_{eff}	—	Effective thermal conductivity coefficient, W m^{-1} K^{-1}
μ	—	Molecular viscosity, Pa·s
d_t	—	Nozzle throat diameter, mm

Abbreviations

AR	—	Area ratio
CFD	—	Computational fluid dynamics
COP	—	Coefficient of performance
MED	—	Multi-effect distillation
NXP	—	Nozzle exit position
TVC	—	Thermal vapor compression

References

[1] I.S. Al-Mutaz, I. Wazeer, Optimization of location of thermocompressor suction in MED-TVC desalination plants, Desal. Water Treat., 57 (2016) 26562–26576.
[2] I.S. Al-Mutaz, I. Wazeer, Current status and future directions of MED-TVC desalination technology, Desal. Water Treat., 55 (2015) 1–9.
[3] H. El-Dessouky, H. Ettouney, I. Alatiqi, G. Al-Nuwaibit, Evaluation of steam jet ejectors, Chem. Eng. Process. Process Intensif., 41 (2002) 551–561.
[4] Y. Zhu, W. Cai, C. Wen, Y. Li, Shock circle model for ejector performance evaluation, Energy Convers. Manage., 48 (2007) 2533–2541.
[5] I.W. Eames, A. Milazzo, D. Paganini, D. Paganini, M. Livi, The design, manufacture and testing of a jet-pump chiller for air conditioning and industrial application, Appl. Therm. Eng., 58 (2013) 234–240.
[6] Y. Yang, S. Shen, S. Zhou, X. Mu, K. Zhang, Research for the adjustable performance of the thermal vapor compressor in the MED-TVC system, Desal. Water Treat., 53 (2015) 1725–1734.
[7] C. Li, Y. Li, W. Cai, Y. Hu, H. Chen, J. Yan, Analysis on performance characteristics of ejector with variable area-ratio for multi-evaporator refrigeration system based on experimental data, Appl. Therm. Eng., 68 (2014) 125–132.
[8] D.T. Chong, M.Q. Hu, W.X. Chen, J.S. Wang, J.P. Liu, J.J. Yan, Experimental and numerical analysis of supersonic air ejector, Appl. Energy, 130 (2014) 679–684.
[9] N.B. Sag, H.K. Ersoy, Experimental investigation on motive nozzle throat diameter for an ejector expansion refrigeration system, Energy Convers. Manage., 124 (2016) 1–12.
[10] W. Fu, Y. Li, Z. Liu, H. Wu, T. Wu, Numerical study for the influences of primary nozzle on steam ejector performance, Appl. Therm. Eng., 106 (2016) 1148–1156.
[11] N. Sharifi, M. Boroomand, An investigation of thermo-compressor design by analysis and experiment: part 1. Validation of the numerical method, Energy Convers. Manage., 69 (2013) 217–227.
[12] N. Sharifi, M. Boroomand, An investigation of thermo-compressor design by analysis and experiment: part 2. Development of design method by using comprehensive characteristic curves, Energy Convers. Manage., 69 (2013) 228–237.
[13] N. Sharifi, S.M.A. Noori Rahim Abadi, R. Kouhikamali, Development of a two-fluid model for predicting phase-changing flows inside thermal vapor compressors used in thermal desalination systems, Appl. Therm. Eng., 195 (2021) 116943, doi: 10.1016/j.applthermaleng.2021.116943.
[14] I.S. Park, Robust numerical analysis based design of the thermal vapor compressor shape parameters for multi-effect desalination plants, Desalination, 242 (2009) 245–255.
[15] N. Ruangtrakoon, S. Aphornratana, T. Sriveerakul, Experimental studies of a steam jet refrigeration cycle: effect of the primary nozzle geometries to system performance, Exp. Therm. Fluid Sci., 35 (2011) 676–683.
[16] N. Ruangtrakoon, T. Thongtip, S. Aphornratana, T. Sriveerakul, CFD simulation on the effect of primary nozzle geometries for a steam ejector in refrigeration cycle, Int. J. Therm. Sci., 63 (2013) 133–145.
[17] J. Liu, L. Wang, L. Jia, X. Wang, The influence of the area ratio on ejector efficiencies in the MED-TVC desalination system, Desalination, 413 (2017) 168–175.
[18] Y. Yang, S. Shen, S. Zhou, R. Liu, H. Yu, Numerical investigation for the supersonic steam jetting flow in the thermal vapor compressor, Desal. Water Treat., 51 (2013) 4684–4693.
[19] H.Q. Wu, Z.L. Liu, B. Han, Y.X. Li, Numerical investigation of the influences of mixing chamber geometries on steam ejector performance, Desalination, 353 (2014) 15–20.

[20] T. Sriveerakul, S. Aphornratana, K. Chunnanond, Performance prediction of steam ejector using computational fluid dynamics: part 2. Flow structure of a steam ejector influenced by operating pressures and geometries, Int. J. Therm. Sci., 46 (2007) 823–833.
[21] C. Qi, X. Wang, H. Feng, Q. Lv, Performance analysis of low-temperature multi-effect distillation system under different feeding modes, Appl. Therm. Eng., 112 (2016) 1452–1459.
[22] J.D. Anderson, Computational Fluid Dynamics: The Basics with Applications, McGraw-Hill, New York, 1995.
[23] Y. Zhu, W. Cai, C. Wen, Y. Li, Numerical investigation of geometry parameters for design of high performance ejectors, Appl. Therm. Eng., 29 (2009) 898–905.
[24] M.K. Ji, T. Utomo, J.S. Woo, Y.H. Lee, H.M. Jeong, H.S. Chung, CFD investigation on the flow structure inside thermo vapor compressor, Energy, 35 (2010) 2694–2702.
[25] K. Ariafar, Performance evaluation of a model thermo-compressor using computational fluid dynamics, Int. J. Mech., 6 (2012) 35–42.
[26] C. Lin, H. Miao, A numerical study on the supersonic steam ejector use in steam turbine system, Math. Probl. Eng., 2013 (2013) 1–9.